






Reconstructing the wave function through the momentum weak value

Junfan Zhu , An Wang , Xiong Liu, Yurong Liu , Zhiyou Zhang *, and Fuhua Gao [†]

College of Physics, Sichuan University, Chengdu 610064, China



(Received 9 May 2021; revised 4 September 2021; accepted 8 September 2021; published 27 September 2021)

The wave function is the cornerstone of quantum mechanics, although it is still open to different interpretations. It has been shown that the amplitude and the phase of a wave function are manifested in the imaginary and real parts of the momentum weak value, respectively. Based on this, we develop a weak measurement scheme to reconstruct the wave function through measuring the momentum weak value. A proof-of-principle experiment is made to confirm the feasibility of our measurement scheme, in which the polarization states and the momentum of light are coupled. We believe the experimental protocol has the potential to be applied in diverse fields such as wave-front sensing, edge detection, and optical communication, and measurement of the momentum weak value may offer valuable insight to better understand quantum mechanics.

DOI: [10.1103/PhysRevA.104.032221](https://doi.org/10.1103/PhysRevA.104.032221)

I. INTRODUCTION

The wave function, which can be also recognized as the quantum state once a representation is chosen, plays a central part in quantum mechanics. According to the Born rule, the squared modulus of the wave function just corresponds to the probability of measuring a particle at a given position (or momentum). However, since the wave function is complex-valued, finding an effective way to measure the amplitude and especially the phase is crucial to capturing the entire information of the wave function. Vogel and Risken showed that the Wigner function can be uniquely determined by tomographic inversion of a large discrete set of measured probability distributions [1]. This method is known as quantum state tomography [2,3]. By performing a Fourier transform on the Wigner function, one can obtain the elements of the density matrix. However, for the ambition of measuring the wave function, quantum state tomography is quite indirect.

Based on the theory of weak measurement, Lundeen *et al.* proposed a scheme in which they can measure the wave function directly [4]. The key element is a sliver that can introduce a weak phase shift in a particular position state where the sliver locates. Although their measurement scheme is ingenious and implementable, there remain two technical problems. An ideal “point filter” is required to be placed in the Fourier transform plane, which brings a lot of difficulties in practice. Because a filter always occupies a certain area, one has to minimize the filter’s size as much as possible to reduce the experimental error. The smaller the filter’s size is, the smaller the probability of a successful detection by the apparatus is, and so the lower the efficiency of measurement is. Moreover, only when the position space is scanned all over, can the entire wave function be obtained. In order to solve these problems, Shi *et al.* came up with a scheme in which

they introduced a weak phase shift in only one momentum state instead of the position states, so that a scan-free measurement can be achieved [5]. Furthermore, since there is no need for a “point filter” to filter out the photons with transversal momentum equal to zero, the efficiency of measurement can be improved a lot. However, a weak phase modulation imposed in only one momentum state is indeed impractical, and due to the periodicity of the sine or cosine function, their scheme may lose its validity in the case where the phase of the wave function is not restricted in the range $[0, 2\pi)$. On the other hand, in notable research, Vallone and Dequal argued that strong measurement gives a better estimation of the wave function [6]. In fact, the only difference of strong and weak measurements is found in the value of the phase shift being weak or $\pi/2$. Therefore, the follow-up studies in Refs. [7–10] were still based on the measurement schemes which were originally proposed by Lundeen *et al.* [4] and Shi *et al.* [5].

Here we develop a different measurement scheme to reconstruct the wave function through the momentum weak value, in which manipulations to only one position or momentum state are no longer required. Then we use a proof-of-principle experiment that is scan-free and diffraction-free to confirm the feasibility of this measurement scheme. A comparison of the two measurement schemes which are respectively proposed by Shi *et al.* and this work is made, indicating that our scheme may prevail in the case where the range of phase is not known beforehand.

This work is organized as follows. In Sec. II, we propose the measurement scheme. In Sec. III, a practical experimental protocol is implemented. In Sec. IV, we make a comparison of the two measurement schemes. Finally a brief conclusion and some discussion are presented in Sec. V.

II. MEASUREMENT SCHEME

Let us consider a pre- and postselected measurement scheme, in which the system is chosen in the state $|\psi_i\rangle$ and the probe is in $|\phi\rangle$, respectively. The unitary transformation,

*zhangzhiyou@scu.edu.cn

[†]gaofuhua@scu.edu.cn

which couples the system and probe, takes the following form [11,12]:

$$U = \exp(-i\gamma\hat{A} \otimes \hat{p}), \quad (1)$$

where γ is defined as the coupling strength, \hat{A} denotes the operator corresponding to the measurable quantity A of the system, and \hat{p} denotes the operator representing the momentum p of the probe. If a two-state system is referred to, \hat{A} is usually chosen as one of the Pauli operators. If we assume that γ is sufficiently weak (a more detailed discussion about how weak γ should be can be found in Ref. [13]), the unitary transformation can be expanded and held up to the first-order term only, namely,

$$U \simeq 1 - i\gamma\hat{A} \otimes \hat{p}. \quad (2)$$

Finally, pre- and postselected measurements are accomplished by a projection at the states $|\psi_f\rangle$ and $|x\rangle$. Hence, the probability distribution function of a successful measurement in the position space is given by

$$\begin{aligned} \Phi(x) &= |\langle x | \langle \psi_f | U | \psi_i \rangle \otimes |\phi \rangle|^2 \\ &\simeq |\langle \psi_f | \psi_i \rangle \phi(x) (1 - i\gamma A_w p_w)|^2, \end{aligned} \quad (3)$$

where $A_w = \frac{\langle \psi_f | \hat{A} | \psi_i \rangle}{\langle \psi_f | \psi_i \rangle}$ is defined as the system weak value, and $p_w = \frac{\langle x | \hat{p} | \phi \rangle}{\langle x | \phi \rangle} = -i \frac{1}{\phi(x)} \frac{\partial \phi(x)}{\partial x}$ is defined as the momentum weak value (here we call p_w the momentum weak value for the purpose of being consistent with previous studies, although “the probe weak value” may be a more appropriate name). With respect to A_w , $|\psi_i\rangle$ and $|\psi_f\rangle$ are the pre- and postselections, while for p_w , $|\phi\rangle$ and $|x\rangle$ play the role of pre- and postselections. It can be noted that the complex-valued p_w carries all the information of the probe wave function, which offers the possibility of reconstructing the wave function through p_w . Because $|\phi\rangle$ is to be measured, the pre- and postselections refer in particular to $|\psi_i\rangle$ and $|\psi_f\rangle$ in the following.

Since $|\phi(x)|^2$ can be readily obtained by a direct measurement of the probability distribution of the wave function and $\langle \psi_f | \psi_i \rangle$ is totally determined by the pre- and postselections, the product $|\langle \psi_f | \psi_i \rangle \phi(x)|^2$ in the second line of Eq. (3) may be considered independent of the reconstruction of the wave function. Then the term unity can be regarded as the background. We can note that A_w can be arbitrarily large by making the pre- and postselections nearly orthogonal, i.e., $\langle \psi_f | \psi_i \rangle \rightarrow 0$. Therefore, although γ is weak, the term $-i\gamma A_w p_w$ can still stand out from the background. This kind of technique is known as weak value amplification. Nearly orthogonal pre- and postselections also lead to an additional reduction of probability, so that practical limitations including noise and saturation of detection can be overcome [14].

For later convenience, let us write the wave function in the form $\phi(x) = a(x) \exp[ib(x)]$, with $a(x)$ being the amplitude and $b(x)$ being the phase. It follows immediately that

$$\text{Re}\{p_w\} = \frac{\partial b(x)}{\partial x} \quad \text{and} \quad \text{Im}\{p_w\} = -\frac{\partial \ln a(x)}{\partial x}, \quad (4)$$

which indicates that the information of the phase and amplitude are contained in the real and imaginary parts of p_w , respectively. Now taking the explicit expression of p_w into

account, Eq. (3) becomes

$$\Phi(x) = \left| \langle \psi_f | \psi_i \rangle a(x) \left[1 - \gamma A_w \frac{\partial \ln a(x)}{\partial x} - i\gamma A_w \frac{\partial b(x)}{\partial x} \right] \right|^2. \quad (5)$$

It can be noted from Eq. (5) that the information of the phase and the information of the amplitude are mixed and then manifested in the probability distribution $\Phi(x)$. Therefore, seeking an effective way to separate the phase and the amplitude is crucial in reconstructing the wave function.

For the particular case where $\langle \psi_f | \psi_i \rangle = 0$, which implies that the pre- and postselections are orthogonal, and $b(x)$ is constant, which implies that the phase is uniformly distributed, Eq. (5) yields

$$\Phi(x) = |\langle \psi_f | \hat{A} | \psi_i \rangle|^2 \left[\gamma \frac{\partial a(x)}{\partial x} \right]^2, \quad (6)$$

indicating a linear relation between the probability distribution and the square of the derivative of the amplitude. On the other hand, when $\langle \psi_f | \psi_i \rangle = 0$ and $a(x)$ is uniformly distributed, it can be given similarly that

$$\Phi(x) = |\langle \psi_f | \hat{A} | \psi_i \rangle|^2 \left[\gamma a \frac{\partial b(x)}{\partial x} \right]^2. \quad (7)$$

Taking advantage of Eqs. (6) and (7), methods for edge detection and phase measurement have been developed, in which the spin-orbit interaction of light has been utilized to build a coupling between spatial and polarization degrees of freedom [15–23]. However, it can be noted that the sign of the derivatives of the amplitude and phase cannot be determined by measuring the probability distribution function. Therefore, Eqs. (6) and (7) can be applied very well in edge detection. But for reconstructing the wave function, they are not sufficient. To solve this problem, Zhu *et al.* found that, by observing the change after introducing a constant bias, the sign of $\partial b(x)/\partial x$ in Eq. (7) can be determined [18]. However, it requires that the intensity of the bias to be at the same order as $a \times \partial b(x)/\partial x$. Then not only can the information of phase can be manifested but also the correct sign can be decided in the mean time. Thus the magnitude of $a \times \partial b(x)/\partial x$ should be *a priori* in practice. Another problem arises in that introducing a bias introduces more or less experimental errors.

Based on Eq. (5), we next develop a measurement scheme in which the information of the amplitude and the information of the phase can be naturally separated without bringing in any other auxiliary experimental setup. First of all, consider that the pre- and postselections are chosen appropriately such that $|\langle \psi_f | \psi_i \rangle|^2$ remains an unchanged value, say μ . This condition may seem to be very strict. However, we show that it can be readily satisfied in our proof-of-principle experiment. Then we make the value of A_w take ν , $-\nu$, $i\nu$, and $-i\nu$, with ν being purely real, respectively. So the corresponding four probability distribution functions are obtained, which may be denoted as $\Phi_1(x)$, $\Phi_2(x)$, $\Phi_3(x)$, and $\Phi_4(x)$. Through straightforward calculation, it can found that

$$\begin{aligned} \Phi_1(x) - \Phi_2(x) &= 4\mu\gamma\nu|\phi(x)|^2 \text{Im}\{p_w\} \\ &= -2\mu\gamma\nu \frac{\partial a^2(x)}{\partial x} \end{aligned} \quad (8)$$

and

$$\begin{aligned}\Phi_3(x) - \Phi_4(x) &= 4\mu\gamma v |\phi(x)|^2 \text{Re}\{p_w\} \\ &= 4\mu\gamma v a^2(x) \frac{\partial b(x)}{\partial x}.\end{aligned}\quad (9)$$

Unlike Eq. (6), Eq. (8) presents a linear relation between the probability difference and the derivative of the square of the amplitude. The sign of $\partial a^2(x)/\partial x$ is automatically determined by two measurements of the probability distribution. It is also worth noting that Eq. (6) only applies for the case where the phase is uniformly distributed. However, Eq. (8) has been derived regardless of the phase distribution, so that a pure measurement of the derivative of the amplitude can be realized. Since $a^2(x)$ is just the probability distribution without pre- and postselections, it can be measured directly. So, actually measurements guided by Eq. (8) are not necessary in reconstructing the wave function; nevertheless, it may have important applications in fields such as edge detection and optical computing. The amplitude $a(x)$ can be obtained immediately once the distribution $a^2(x)$ is given.

Equation (9) shows that the information of the amplitude and the information of the phase are together manifested in the probability difference. This is understandable, since only when the amplitude is not zero can the definition of the phase makes sense. However, as stated in the previous paragraph, $a^2(x)$ can be measured directly. Therefore, the information of the phase can readily be separated from that of the amplitude. It can be also noted that if we replace $b(x)$ with $b(x) + b_0$, where b_0 is a constant, Eq. (9) remains invariant. This invariance corresponds to the fact that the probability is symmetric under a U(1) transformation imposed on the wave function. Henceforth, there must be some boundary conditions if we are pursuing a definite phase distribution.

When we refer to the wave function in one dimension, $b(x)$ can be derived by a simple integral calculation once $\partial b(x)/\partial x$ is obtained. The constant term brought by the integral can be determined by the boundary conditions that

$$\lim_{x \rightarrow \pm\infty} b(x) = 0. \quad (10)$$

For the two-dimensional wave function, in addition to $\partial b(x, y)/\partial x$, the derivative with respect to the y direction, say $\partial b(x, y)/\partial y$, is also required. Then, by utilizing the Fourier reconstruction algorithm, the phase distribution can be given by (see Appendix A)

$$b(x, y) = \mathcal{F}^{-1} \left\{ \mathcal{F} \left[\frac{\partial b(x, y)}{\partial x} + i \frac{\partial b(x, y)}{\partial y} \right] / (ip_x - p_y) \right\}, \quad (11)$$

where p_x and p_y denote momenta corresponding to x and y , and \mathcal{F} and \mathcal{F}^{-1} represent the Fourier and inverse Fourier transforms, respectively. When Eq. (11) is applied, it has already been implied that there hold the boundary conditions that

$$\lim_{x, y \rightarrow \pm\infty} b(x, y) = 0. \quad (12)$$

Consequently, because $a^2(x)$ can be measured directly and $\partial b(x)/\partial x$ can be obtained by two measurements guided by Eq. (9), the wave function can be reconstructed. We note

that the measurement scheme presented here has already been applied, in part, in work by Yang *et al.*, in which a birefringent crystal coupled the polarization states and the momentum [24]. However, they did not notice that the momentum weak value is actually complex-valued. Furthermore, diffraction of light in the pre- and postselected measurements was not taken into account. As a result, the wave functions reconstructed were not completely accurate.

III. PROOF-OF-PRINCIPLE EXPERIMENT

In order to implement the measurement scheme given in Sec. II, a proof-of-principle experiment to reconstruct a photonic wave function is made, the schematic diagram of which is depicted in Fig. 1. A monochromatic light beam with a wavelength of $\lambda = 632.8$ nm is generated by a He-Ne laser. Then the light beam is expanded by a telescope system consisting of lenses 1 and 2. Afterwards, in the 4f imaging system between lenses 3 and 4, the pre- and postselected measurements are performed. In the end, the beam profiler (BP) placed in the back focal plane of lens 4 detects the intensity distribution which corresponds to the wave function $\phi(x, y)$ of photons in the front focal plane of lens 3.

In the pre- and postselected measurements, the first polarizer (P1) with the polarization direction set at $\pi/4$ preselects photons in the state

$$|\psi_i\rangle = \frac{1}{\sqrt{2}}(|H\rangle + |V\rangle), \quad (13)$$

where $|H\rangle$ and $|V\rangle$ denote the horizontal and vertical polarization states, respectively. The Wollaston prism (WP) that is placed in the confocal plane couples the Pauli operator

$$\hat{A} = |H\rangle\langle H| - |V\rangle\langle V| \quad (14)$$

and the momentum (see Appendix B). The coupling strength can be adjusted by changing the length-width ratio of the WP or the incident angle of the light beam on the WP. As shown in Fig. 1, the WP can be rotated to achieve a directional conversion of the momentum to be coupled. Then a quarter wave plate (QWP) together with the second polarizer (P2) postselect photons in the state [25]

$$|\psi_f\rangle = \frac{1}{\sqrt{2}}[\exp(-i\varepsilon)|H\rangle - \exp(i\varepsilon)|V\rangle], \quad (15)$$

with ε being the angle at which the polarization direction of P2 deviates from $-\pi/4$. So it can be obtained immediately that $\mu = \sin^2 \varepsilon$ and $A_w = -i \cot \varepsilon$. By rotating the angle to $\pm\varepsilon$, respectively, a reconstruction of the phase which is indicated by Eq. (9) can be realized. It should be noted that the 4f imaging system guarantees what the BP detects is exactly corresponding to $\phi(x, y)$. In other words, our experimental protocol is diffraction-free.

We first characterize photons with a Gaussian distribution in the transverse position space. When we make the polarization directions of P1 and P2 parallel to each other, it turns out that $\varepsilon = \pi/2$ and so $A_w = 0$. Under this circumstance, $a^2(x, y)$ can be directly read out in the BP according to Eq. (5). The distribution of $a^2(x, y)$ is shown in Fig. 2(a). Since in this work what we care about most is the distribution instead of the absolutely accurate values of $a(x, y)$ and $b(x, y)$, all figures

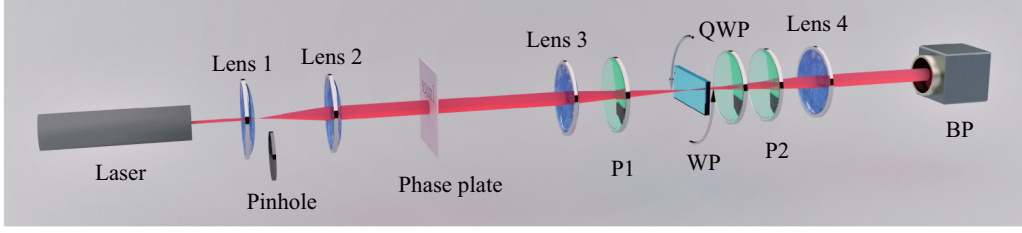


FIG. 1. Experimental implementation of the photonic wave-function reconstruction. The laser generates a monochromatic Gaussian-distributed light beam. Lenses 1 and 2 form a telescope system, in the confocal plane of which a pinhole can be plugged in to generate a wave whose amplitude is approximately uniform. Lenses 3 and 4 construct a 4f system, in which weak measurement is performed. Polarizer 1 (P1) plays the role of the preselection. A quarter wave plate (QWP) and the other polarizer, polarizer 2 (P2), postselect the polarization system. A Wollaston prism (WP) builds a coupling between the momentum and the polarization degrees of freedom. A beam profiler (BP) detects the intensity distribution.

about distribution will be normalized first and then presented henceforth. After the polarization direction of P2 being rotated to be perpendicular to P1's, measurements of the phase get started. We fine-tune the value of ε to take ± 0.05 rad, so that the distribution functions $\Phi_3(x, y)$ and $\Phi_4(x, y)$ can be obtained. The difference of $\Phi_3(x, y)$ and $\Phi_4(x, y)$ is presented in Fig. 2(b). As a result, $b(x, y)$ can be reconstructed, which is given in Fig. 2(c). For a better visual presentation, here we plot $-b(x, y)$ instead of $b(x, y)$. It can be seen that the phase distribution, especially the parts of the edge, is not very symmetric. The reason may be twofold: First, the Gaussian beam generated is not perfectly symmetric. Second, an optical system is always diffraction-limited in practice.

In order to verify the correctness of our reconstructed phase, we plot the distribution of $\partial b(x, 0)/\partial x$ in Fig. 2(d). Since under the paraxial assumption, the surfaces of the

constant phase of a Gaussian beam can be approximately considered spherical, the phase distribution in the front focal plane of lens 3 may be given by [26]

$$b(x, y) \simeq \frac{2\pi}{\lambda} \left(z_0 + \frac{x^2 + y^2}{2z_0} \right), \quad (16)$$

where z_0 is the distance from the waist to the focal plane. So it follows at once the relation $\partial b(x, 0)/\partial x \propto x$. The linearly fitting line is plotted in Fig. 2(d) as well. We can see that the fitting line does not match perfectly well with the experimental results for the case where $x > 0$. Nevertheless, since the coefficient of determination $R^2 = 0.9918$, which is very closed to unity, the reconstructed phase is convincing to be considered correct.

Compared to the phase, measuring the amplitude is rather trivial. Hence, by inserting a pinhole in the confocal plane of lenses 1 and 2, we generate a light beam whose amplitude is approximately uniform to reconstruct a phase-only distribution placed in the front focal plane of lens 3. The pattern of the transmission-type phase plate is a four-leaf clover, which is manufactured by covering a cloverlike mask on a quartz substrate and then coating the other parts of the substrate with SiO_2 . The depth of the concave clover is about 500 nm. We plot $\partial b(x, y)/\partial x$ and $\partial b(x, y)/\partial y$ in Figs. 3(a) and 3(b), respectively. It can be seen that, in the light spot, the parts apart from the edges of the clover are not all equal to zero. This is because even after being filtered by a pinhole, the phase distribution of photons is not uniform, which can be confirmed by the phase distribution reconstructed without the cloverlike phase plate shown in Fig. 3(c). Finally, the phase distribution with the clover is presented in Fig. 3(d). For better visual presentations, we also plot $-b(x, y)$ instead of $b(x, y)$.

IV. COMPARISON OF THE TWO MEASUREMENT SCHEMES

In this section, we theoretically compare the measurement scheme proposed by Shi *et al.* [5] with the one presented in Sec. II. For an intuitive understanding, we also consider reconstructing the photonic wave function.

Suppose an evolution $\exp(-i\alpha\hat{A}) \in \text{SU}(2)$ is implemented in the state $|p_0\rangle$, where $\exp(-i\alpha\hat{A})$ indicates a rotation about the axis \hat{A} by an angle 2α . If we take $\hat{A} = |H\rangle\langle H| - |V\rangle\langle V|$, then $\exp(-i\alpha\hat{A})$ induces a phase difference of 2α between

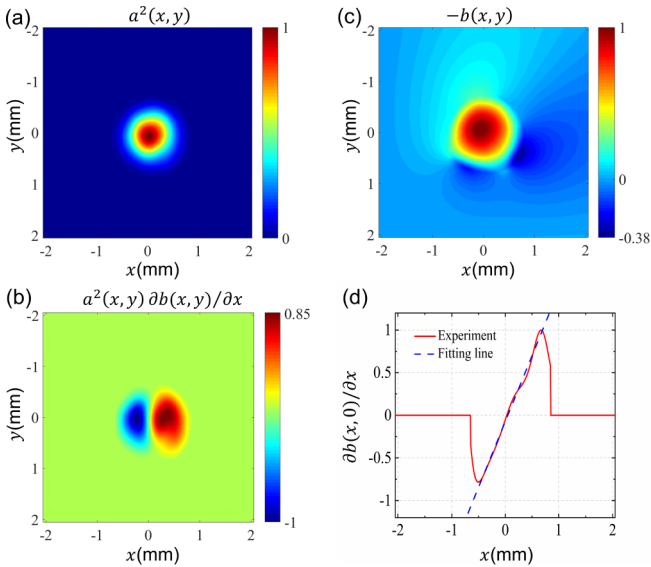


FIG. 2. Experimental results of the Gaussian-distributed photons. (a) The probability distribution $a^2(x, y)$. (b) The distribution $a^2(x, y) \frac{\partial b(x, y)}{\partial x}$ about the amplitude and the phase, which is obtained by calculating the difference of $\Phi_3(x, y)$ and $\Phi_4(x, y)$. (c) The reconstructed phase distribution $-b(x, y)$. (d) $\frac{\partial b(x, 0)}{\partial x}$ in a function of x . The red curve corresponds to the experimental results, and the blue dotted line corresponds to the fitting line.

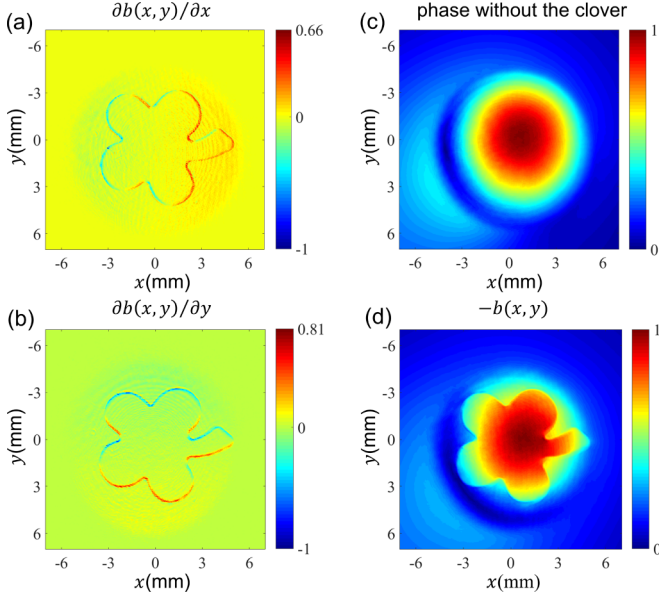


FIG. 3. Experimental results of the cloverlike phase-only-distributed photons. (a) The derivative of the phase with respect to x , $\frac{\partial b(x,y)}{\partial x}$. (b) The derivative of the phase with respect to y , $\frac{\partial b(x,y)}{\partial y}$. (c) The reconstructed phase distribution without the cloverlike phase plate. (d) The reconstructed phase distribution with the cloverlike phase plate, $-b(x,y)$.

the polarization states $|H\rangle$ and $|V\rangle$. For other states $|p_k\rangle$ with the index k running all over the momentum space except for $k = 0$, no evolution is implemented. In this case, the unitary transformation is given by

$$\begin{aligned}
 U_s &= \exp(-i\alpha\hat{A}) \otimes |p_0\rangle\langle p_0| + \sum_{k \neq 0} |p_k\rangle\langle p_k| \\
 &= \left[1 + \sum_{n=1}^{\infty} \frac{1}{n!} (-i\alpha\hat{A})^n \right] \otimes |p_0\rangle\langle p_0| + \sum_{k \neq 0} |p_k\rangle\langle p_k| \\
 &= 1 + \sum_{n=1}^{\infty} \frac{1}{n!} (-i\alpha\hat{A})^n \otimes |p_0\rangle\langle p_0| \\
 &= \exp(-i\alpha\hat{A} \otimes |p_0\rangle\langle p_0|),
 \end{aligned} \tag{17}$$

where in the second line we have applied the Taylor formula, and in the third line the completeness relation $\sum_k |p_k\rangle\langle p_k| = 1$ has been used. U_s is equivalent to the unitary transformation adopted by Shi *et al.* [5], which couples the Pauli operator of polarization and the zero-momentum state.

On the other hand, let us consider a case where an evolution $\exp(-i\beta\hat{p})$ is implemented on the state $|H\rangle$ while the other evolution $\exp(i\beta\hat{p})$ is implemented on $|V\rangle$. We note that $\exp(-i\beta\hat{p})$ is the so-called displacement operator, whose function can be manifested in the following relation:

$$\langle x | \exp(-i\beta\hat{p}) | \phi \rangle = \phi(x - \beta). \tag{18}$$

So, $\exp(-i\beta\hat{p})$ acts on every position state instead of on one particular position state. In this case, the unitary transforma-

tion is given by

$$\begin{aligned}
 U_z &= \exp(-i\beta\hat{p}) \otimes |H\rangle\langle H| + \exp(i\beta\hat{p}) \otimes |V\rangle\langle V| \\
 &= \sum_{n=0}^{\infty} \frac{1}{n!} (-i\beta\hat{p})^n \otimes (|H\rangle\langle H| + (-1)^n |V\rangle\langle V|) \\
 &= \exp(-i\beta\hat{A} \otimes \hat{p}),
 \end{aligned} \tag{19}$$

where the relation $\hat{A}^{2n} = 1$ has been implied in the third line. U_z is just the unitary transformation adopted in Sec. II, which couples the Pauli operator and the momentum.

Therefore, the essential difference between the two measurement schemes is the evolution. $\exp(-i\alpha\hat{A})$ acts on the zero-momentum state $|p_0\rangle$, which is actually impossible to realize in practice. Shi *et al.* [5] took an area of 2-by-2 pixels of a Spatial Light Modulator (SLM) as $|p_0\rangle\langle p_0|$ in an approximate way. There is no doubt that $\exp(-i\alpha\hat{A}) \otimes |p_0\rangle\langle p_0|$ can be realized as much as possible with the size of each pixel getting smaller, which is, however, technically difficult to achieve. As for our scheme, $\exp(-i\beta\hat{p})$ acts on the polarization state $|H\rangle$ while $\exp(i\beta\hat{p})$ acts on $|V\rangle$, which can be readily realized by a birefringent crystal without any compromise in technique.

If α is sufficiently weak such that $\exp(-i\alpha\hat{A})$ can be expanded and held up to the first-order term only, then the zero-momentum-state weak value can be naturally defined by

$$\langle \pi_{p_0} \rangle_w = \frac{\langle x | p_0 \rangle \langle p_0 | \phi \rangle}{\langle x | \phi \rangle} = \frac{c}{\phi(x)}, \tag{20}$$

where c is a constant that can be determined through normalization. Since c is complex-valued, we further write $c = c_1 + ic_2$ henceforth. Taking $\phi(x) = a(x) \exp[ib(x)]$ into account, it follows at once that

$$\begin{aligned}
 \text{Re}\{\langle \pi_{p_0} \rangle_w\} &= c_1 \frac{\cos[b(x)]}{a(x)} + c_2 \frac{\sin[b(x)]}{a(x)}, \\
 \text{Im}\{\langle \pi_{p_0} \rangle_w\} &= c_2 \frac{\cos[b(x)]}{a(x)} - c_1 \frac{\sin[b(x)]}{a(x)}.
 \end{aligned} \tag{21}$$

The momentum weak value p_w has already been given by Eq. (4). Different from the case of p_w , the information of the phase and the information of the amplitude are contained in both the real and imaginary parts of $\langle \pi_{p_0} \rangle_w$. Each of $\text{Re}\{\langle \pi_{p_0} \rangle_w\}$ and $\text{Im}\{\langle \pi_{p_0} \rangle_w\}$ can be obtained by two corresponding measurements [5].

Assume that $a(x)$ is constant and difficulties brought by the Fourier reconstruction algorithm are disregarded for simplicity. We can consider $\cos[b(x)]$ and $\sin[b(x)]$ as two quantities which can be obtained by Eq. (21). Then $\tan[b(x)]$ can be calculated to uniquely determine $b(x)$, since $\tan[b(x)]$ is bijective when $b(x) \in [0, 2\pi)$. For the case where $b(x)$ is not restricted in $[0, 2\pi)$, $b(x)$ cannot be settled unless some other technical methods, such as the phase unwrapping algorithm, are introduced. For reconstructing a one-dimensional phase distribution through $\text{Re}\{p_w\}$, two measurements are already sufficient. For the two-dimensional case, four measurements are also required. However, there will be no restriction to the range of $b(x)$. Hence, if we refer to a wave function with the range of phase completely unknown, making use of p_w to reconstruct it can prevail over the case where $\langle \pi_{p_0} \rangle_w$ is applied.

V. CONCLUSION AND DISCUSSION

In conclusion, the information of the phase and the information of the amplitude of a wave function are contained in the real and imaginary parts of the momentum weak value, respectively. Thus we have proposed a weak measurement scheme to separate the phase and the amplitude from the probability distribution functions. Then, with the principle that the amplitude distribution can be measured directly and the phase distribution can be recovered by the Fourier reconstruction algorithm, the wave function can be reconstructed. In order to show the feasibility of the measurement scheme, we have made a proof-of-principle experiment. At last, a comparison of our measurement scheme and the one proposed by Shi *et al.* [5] has been made, in which we have found that our measurement scheme may be preferable in the case where the range of phase is unknown.

Since optical experiments can be implemented well and photons can be readily prepared in the same quantum state, we have chosen to reconstruct the photonic wave function. However, it should be noted that the wave function of other kinds of particles, such as neutrons, can be also measured by this method, although this may be beyond the reach of current technology. Taking a beam of neutrons, for example, a coupling between the Pauli operator of spin and the position can be built by imposing a slowly varying magnetic field [11], which offers the possibility to realize the wave function reconstruction of neutrons.

We also notice that the momentum weak value, combined with the introduction of a global random variable, can define the epistemically restricted phase-space (ERPS) distribution [27]. The real and imaginary parts of the momentum weak value correspond to the position-dependent average and variance of the epistemically restricted momentum fluctuation, respectively. We may consider that the randomness in each quantum measurement is due to the random fluctuation of the epistemically restricted momentum. Therefore, our measurement scheme provides a realistic way to obtain the restricted momentum field and study the ERPS representation.

ACKNOWLEDGMENTS

This work is supported by the Natural Science Foundation of China (Grant No. 11674234), the Science Specialty Program of Sichuan University (Grant No. 2020SCUNL210).

APPENDIX A: FOURIER RECONSTRUCTION ALGORITHM

For a real and normalized distribution function $f(x, y)$ which is square-integrable on $(-\infty, +\infty)$, we have

$$\iint_{-\infty}^{+\infty} dx dy f(x, y) = 1. \quad (\text{A1})$$

And $f(x, y)$ should satisfy the boundary conditions

$$\lim_{x, y \rightarrow \pm\infty} f(x, y) = 0. \quad (\text{A2})$$

On this basis, we introduce the following equation:

$$\begin{aligned} & \iint_{-\infty}^{+\infty} dx dy \frac{\partial}{\partial x} f(x, y) e^{-i(xp_x + yp_y)} \\ &= \iint_{-\infty}^{+\infty} dx dy \left[\frac{f(x, y)}{\partial x} - ip_x f(x, y) \right] e^{-i(xp_x + yp_y)}. \end{aligned} \quad (\text{A3})$$

According to the boundary conditions above, the left-hand side of Eq. (A3) should be zero. So, it follows that

$$ip_x \mathcal{F}[f(x, y)] = \mathcal{F}\left[\frac{\partial f(x, y)}{\partial x}\right], \quad (\text{A4})$$

where \mathcal{F} denotes the two-dimensional Fourier transform. Up to this point, one may conclude that

$$f(x, y) = \mathcal{F}^{-1}\left\{\mathcal{F}\left[\frac{\partial f(x, y)}{\partial x}\right] / ip_x\right\}. \quad (\text{A5})$$

However, since in numerical computation $\mathcal{F}\left[\frac{\partial f(x, y)}{\partial x}\right]$ usually cannot be zero where p_x is equal to zero, $p_x = 0$ will behave like a “singular line.” Therefore, we can introduce another equation:

$$-p_y \mathcal{F}[f(x, y)] = \mathcal{F}\left[i \frac{\partial f(x, y)}{\partial y}\right]. \quad (\text{A6})$$

Combining Eqs. (A4) and (A6), it can be concluded that

$$f(x, y) = \mathcal{F}^{-1}\left\{\mathcal{F}\left[\frac{\partial f(x, y)}{\partial x} + i \frac{\partial f(x, y)}{\partial y}\right] / (ip_x - p_y)\right\}, \quad (\text{A7})$$

which is just the Fourier reconstruction algorithm used in this work. Now it can be noted that there is only one singularity where $p_x = 0$ and $p_y = 0$. By setting a high-pass filter before the inverse Fourier transform, the problem caused by the singularity can be solved.

APPENDIX B: HOW DOES THE WOLLASTON PRISM CONSTRUCT THE COUPLING?

First of all, we need to be clear about one thing, that at the waist of a Gaussian beam, the wave front becomes a plane. The functional diagram of the Wollaston prism (WP) is given in Fig. 4. It can be readily derived from Snell’s law that

$$\begin{aligned} n_o \sin \theta &= n_e \sin(\theta + \alpha_1), \\ n_e \sin \theta &= n_o \sin(\theta - \alpha_2), \end{aligned} \quad (\text{B1})$$

where n_o and n_e denote the refractive indices of the so-called ordinary light (O-light) and extraordinary light (E-light), respectively. Then the solutions are given by

$$\begin{aligned} \alpha_1 &= \arcsin\left(\frac{n_o}{n_e} \sin \theta\right) - \theta, \\ \alpha_2 &= \theta - \arcsin\left(\frac{n_e}{n_o} \sin \theta\right). \end{aligned} \quad (\text{B2})$$

The distance of the O-light and E-light emergent is given by

$$\delta_x = h(\tan \alpha_1 + \tan \alpha_2). \quad (\text{B3})$$

The length of the WP is so tiny that δ_x can be considered as a second-order small value and then be neglected. Applying

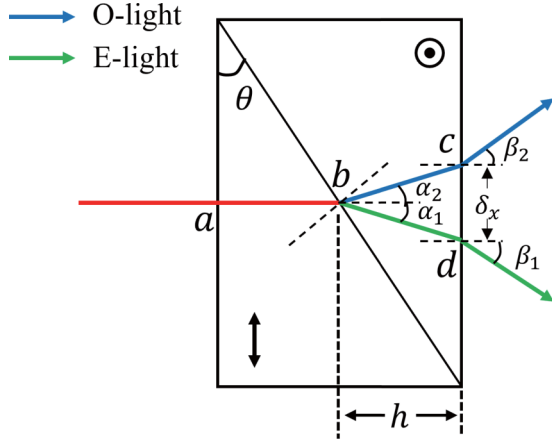


FIG. 4. The functional diagram of the Wollaston prism.

Snell's law again, the following emergent angles can be obtained:

$$\begin{aligned}\beta_1 &= \arcsin[\tan \theta (n_o - n_e \cos \alpha_1)], \\ \beta_2 &= \arcsin[\tan \theta (n_o \cos \alpha_2 - n_e)].\end{aligned}\quad (\text{B4})$$

Since θ is made sufficiently small, α_1 and α_2 can be considered small as well. It finally turns out that

$$\gamma \equiv \beta_1 \approx \beta_2 \approx \arcsin[\tan \theta (n_o - n_e)]. \quad (\text{B5})$$

Recalling that at the waist we can consider there is a transformation from the position space to the momentum space. Thus the wave function of the O-light and E-light emergent reads $\exp(-i\gamma p_x) \otimes |H\rangle\langle H| + \exp(i\gamma p_x) \otimes |V\rangle\langle V|$, which can be written symbolically as

$$U = \exp(-i\gamma \hat{A} \otimes \hat{p}_x), \quad (\text{B6})$$

with $\hat{A} = |H\rangle\langle H| - |V\rangle\langle V|$.

If the light beam is not incident perpendicularly, it can be readily found that γ will be also dependent on the incident angle.

The phase difference between the O-light and the E-light, which is denoted as φ , can be given by

$$\varphi = \frac{2\pi}{\lambda} [(n_e - n_o)\overline{ab} + (n_o\overline{bc} - n_e\overline{bd})], \quad (\text{B7})$$

where \overline{ab} is the length between points a and b , etc. The effect of this phase difference can be described by a unitary transformation:

$$U_{\text{ph}} = \exp(-i\varphi \hat{A}/2). \quad (\text{B8})$$

We can put U_{ph} and the postselection $|\psi_f\rangle$ together to form a new postselection as follows:

$$U_{\text{ph}}^\dagger |\psi_f\rangle = \frac{1}{\sqrt{2}} [e^{-i(\varepsilon - \frac{\varphi}{2})} |H\rangle - e^{i(\varepsilon - \frac{\varphi}{2})} |V\rangle]. \quad (\text{B9})$$

In the experiment, we found that φ can range from 0 to 2π by choosing different incident points on the WP. So, before the measurement of the wave function, a particular incident point was set, in which $\varphi = 0$.

-
- [1] K. Vogel and H. Risken, Determination of quasiprobability distributions in terms of probability distributions for the rotated quadrature phase, *Phys. Rev. A* **40**, 2847 (1989).
 - [2] D. T. Smithey, M. Beck, M. G. Raymer, and A. Faridani, Measurement of the Wigner Distribution and the Density Matrix of a Light Mode Using Optical Homodyne Tomography: Application to Squeezed States and the Vacuum, *Phys. Rev. Lett.* **70**, 1244 (1993).
 - [3] G. Breitenbach, S. Schiller, and J. Mlynek, Measurement of the quantum states of squeezed light, *Nature (London)* **387**, 471 (1997).
 - [4] J. S. Lundeen, B. Sutherland, A. Patel, C. Stewart, and C. Bamber, Direct measurement of the quantum wavefunction, *Nature (London)* **474**, 188 (2011).
 - [5] Z. Shi, M. Mirhosseini, J. Margiewicz, M. Malik, F. Rivera, Z. Zhu, and R. W. Boyd, Scan-free direct measurement of an extremely high-dimensional photonic state, *Optica* **2**, 388 (2015).
 - [6] G. Vallone and D. Dequal, Strong Measurements Give a Better Direct Measurement of the Quantum Wave Function, *Phys. Rev. Lett.* **116**, 040502 (2016).
 - [7] C.-R. Zhang, M.-J. Hu, Z.-B. Hou, J.-F. Tang, J. Zhu, G.-Y. Xiang, C.-F. Li, G.-C. Guo, and Y.-S. Zhang, Direct measurement of the two-dimensional spatial quantum wave function via strong measurements, *Phys. Rev. A* **101**, 012119 (2020).
 - [8] G. S. Thekkadath, L. Giner, Y. Chalich, M. J. Horton, J. Banker, and J. S. Lundeen, Direct Measurement of the Density Matrix of a Quantum System, *Phys. Rev. Lett.* **117**, 120401 (2016).
 - [9] M. Malik, M. Mirhosseini, M. P. J. Lavery, J. Leach, M. J. Padgett, and R. W. Boyd, Direct measurement of a 27-dimensional orbital-angular-momentum state vector, *Nat. Commun.* **5**, 3115 (2014).
 - [10] C.-R. Zhang, M.-J. Hu, G.-Y. Xiang, Y.-S. Zhang, C.-F. Li, and G.-C. Guo, Direct strong measurement of a high-dimensional quantum state, *Chin. Phys. Lett.* **37**, 080301 (2020).
 - [11] Y. Aharonov, D. Z. Albert, and L. Vaidman, How the Result of a Measurement of a Component of the Spin of a Spin-1/2 Particle can Turn Out to be 100, *Phys. Rev. Lett.* **60**, 1351 (1988).
 - [12] A. G. Kofman, S. Ashhab, and F. Nori, Nonperturbative theory of weak pre- and post-selected measurements, *Phys. Rep.* **520**, 43 (2012).
 - [13] J. Zhu, Z. Li, Y. Liu, Y. Ye, Q. Ti, Z. Zhang, and F. Gao, Weak measurement with the peak-contrast-ratio pointer, *Phys. Rev. A* **103**, 032212 (2021).
 - [14] L. Xu, Z. Liu, A. Datta, G. C. Knee, J. S. Lundeen, Y.-q. Lu, and L. Zhang, Approaching Quantum-Limited Metrology with Imperfect Detectors by Using Weak-Value Amplification, *Phys. Rev. Lett.* **125**, 080501 (2020).
 - [15] J. Zhou, H. Qian, C.-F. Chen, J. Zhao, G. Li, Q. Wu, H. Luo, S. Wen, and Z. Liu, Optical edge detection based on high-efficiency dielectric metasurface, *Proc. Natl. Acad. Sci. USA* **116**, 11137 (2019).
 - [16] J. Zhou, S. Liu, H. Qian, Y. Li, H. Luo, S. Wen, Z. Zhou, G. Guo, B. Shi, and Z. Liu, Metasurface enabled quantum edge detection, *Sci. Adv.* **6**, eabc4385 (2020).

- [17] T. Zhu, Y. Lou, Y. Zhou, J. Zhang, J. Huang, Y. Li, H. Luo, S. Wen, S. Zhu, Q. Gong, M. Qiu, and Z. Ruan, Generalized Spatial Differentiation from the Spin Hall Effect of Light and Its Application in Image Processing of Edge Detection, *Phys. Rev. Appl.* **11**, 034043 (2019).
- [18] T. Zhu, J. Huang, and Z. Ruan, Optical phase mining by adjustable spatial differentiator, *Adv. Photonics* **2**, 016001 (2020).
- [19] J. Huang, T. Zhu, and Z. Ruan, Two-Shot Calibration Method for Phase-Only Spatial Light Modulators with Generalized Spatial Differentiator, *Phys. Rev. Appl.* **14**, 054040 (2020).
- [20] T. Zhu, C. Guo, J. Huang, H. Wang, M. Orenstein, Z. Ruan, and S. Fan, Topological optical differentiator, *Nat. Commun.* **12**, 680 (2021).
- [21] S. He, J. Zhou, S. Chen, W. Shu, H. Luo, and S. Wen, Spatial differential operation and edge detection based on the geometric spin Hall effect of light, *Opt. Lett.* **45**, 877 (2020).
- [22] S. He, J. Zhou, S. Chen, W. Shu, H. Luo, and S. Wen, Wavelength-independent optical fully differential operation based on the spin-orbit interaction of light, *APL Photonics* **5**, 036105 (2020).
- [23] D. Xu, S. He, J. Zhou, S. Chen, S. Wen, and H. Luo, Optical analog computing of two-dimensional spatial differentiation based on the Brewster effect, *Opt. Lett.* **45**, 6867 (2020).
- [24] M. Yang, Y. Xiao, Y.-W. Liao, Z.-H. Liu, X.-Y. Xu, J.-S. Xu, C.-F. Li, and G.-C. Guo, Zonal reconstruction of photonic wavefunction via momentum weak measurement, *Laser Photonics Rev.* **14**, 1900251 (2020).
- [25] X. Qiu, L. Xie, X. Liu, L. Luo, Z. Li, Z. Zhang, and J. Du, Precision phase estimation based on weak-value amplification, *Appl. Phys. Lett.* **110**, 071105 (2017).
- [26] W. Nagourney, *Quantum Electronics for Atomic Physics and Telecommunication* (Oxford University, Oxford, 2014).
- [27] A. Budiyono, Epistemically restricted phase-space representation, weak momentum value, and reconstruction of the quantum wave function, *Phys. Rev. A* **100**, 032125 (2019).